ARTICLE

Comparison of Ligands in Palladium-catalyzed Electrochemical Allyl 4-Pyridinylation

Wei-Jie Ding [a,b,*], Chun-Hui Yang [b], Zhong-Tao Feng [c], Shi-Rong Lu [a], Xu Cheng [b,*]

[a] Department of Material Science and Technology, Taizhou University, Taizhou 318000, Zhejiang, China
[b] School of Chemistry and Chemical Engineering Nanjing University, Nanjing 210023, Jiangsu, China
[c] School of Chemistry, Chemical Engineering and Biotechnology, Nanyang Technological University, Singapore 637371, Singapore

Abstract

4-CN-pyridine is a widely applied 4-pyridinylation reagent for diverse transformations. Conventionally, the reaction proceeds via an open-shell radical cross-coupling pathway. Following our previous study, in this work, we report the Pd-catalyzed allyl 4-pyrinylation reaction under electrochemical conditions. The reaction proceeds via radical-polar crossover pathway in which the role of phosphine ligand in reactivity and selectivity was extensively investigated.

Keywords: Electrochemistry; Palladium; Phosphine; Pyridinylation; Allyl

1. Introduction

The pyridine group could give a molecule additional hydrophilicity with decent stability toward oxidation conditions. Pyridine is the mostly applied aromatic heterocycle in pharmaceutical products [1]. Among the various protocols used to introduce pyridine moieties into carbon skeletons, the pyridinylation with 4-CN-pyridine is highly efficient (Scheme 1a) [2]. Typically, 4-CN pyridine undergoes radical pathway via an persistent radical intermediate **A**, which reacts with a number of counterparts to give various formal-pyridine adducts. To date, the substrate scope has covered Csp3-H [3−7], nucleophilic reagents [8], carboxylic acid [9−11] ketones [12−14], alkenes [15−18], -unsaturated compounds [19−22], amines [23], and imines [24,25]. Due to the persistence of the radical intermediate, 4-CN-pyrdine can be activated under thermal, photoredox, and electrochemical conditions. On the other hand, the adoption of this persistent radical into the close-shell reaction pathway is still a challenge.

The catalytic trapping of open shell intermediates is well established via diverse transition metal catalysts [26−30]. One successful protocol is the radical rebound sequence, in which a radical species receives one electron from transition metal complex, forming anionic ligand and coordinating to the metal center [31−34]. This process achieved the control of chemo-, regio- and enantioselectivity by merge of the transition metal catalysis and radical chemistry. In 2022, we reported the first Pd-catalyzed asymmetric allyl pyridinylation reaction [35]. In that work, the 4-CN-pyridine was used as the pyridinylation reagent driven by electricity. Instead of direct cathodic reduction of 4-CN-pyridine to persistent radicals, the Pd-allyl complex shuttles electrons from the cathode to 4-CN-pyridine, and captures the generated persistent radicals via rebound. With (R)-DTBM-SEGPHOS as the chiral ligand, the Pd complex could lead to the reductive elimination of the capture pyridine and allyl group to furnish the chiral allyl pyridine product with excellent enantioselectivity in good yield. Instead

Received 14 August 2023; Received in revised form 4 September 2023; Accepted 8 December 2023
Available online 24 December 2023

* Corresponding author, Wei-Jie Ding, Tel.: (86-576)88662365, E-mail address: wding@tzc.edu.cn.
* Corresponding author, Xu Cheng, Tel: (86-25)89699037, E-mail address: chengxu@nju.edu.cn.

https://doi.org/10.61558/2993-074X.3438

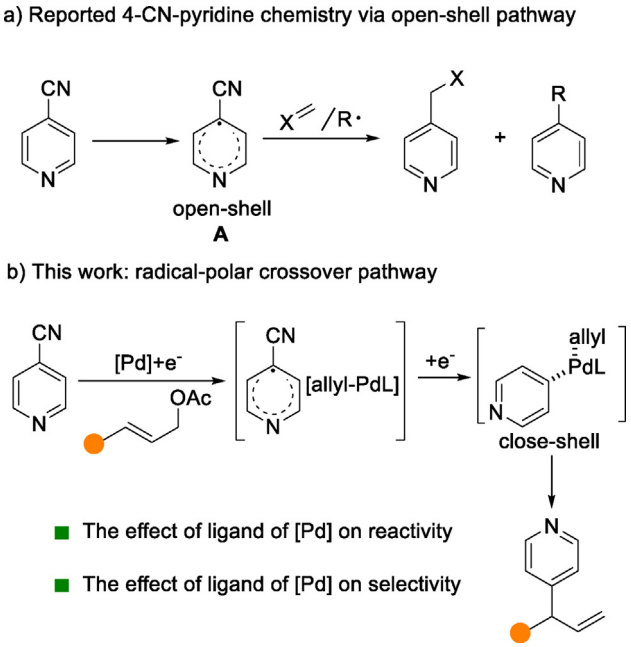

Scheme 1. The 4-CN-pyridine reaction as open/close shell pyridinylation reagent.

of radical cross-coupling, 4-CN-pyridine underwent a radical-polar crossover pathway [36–38]. It was found that the chiral diphosphine ligand plays an essential role in the Pd-catalyzed allyl substitution under redox conditions by Mei [39], Yu [40–42] and us. This observation prompted us to study the effects of P ligands with diverse steric and electronic features on the electrochemical reaction outcome with yield as the benchmark in this work (Scheme 1b).

2. Experimental section

A 10 mL three-necked flask was charged with $PdCl_2$ (0.02 mmol, 10 mol%) and dppp (0.024 mmol, 12 mol%). The flask was evacuated and backfilled with argon three times, and anhydrous MeCN (3 mL) was added via syringe. The mixture was stirred at room temperature for 0.5 hours. Then, the substrates **1a** (0.2 mmol, 1.0 equiv) and **2a** (0.6 mmol, 3.0 equiv), and nBu$_4$NBF$_4$ (0.1 mmol, 0.5 equiv.) were added. The flask was equipped with graphite felt as the cathode and zinc as the anode. The zinc anode was attached to a platinum wire, and the graphite felt cathode was attached to a titanium wire. The flask was evacuated and backfilled with argon three times, and anhydrous MeCN (2 mL) and MeOH (1 mL) were added via syringe. The mixture was stirred at room temperature and constant current electrolysis (20 mA). After the reaction was completed (TLC or GC-MS analysis, approximately 4 hours), the mixture was extracted with ethyl acetate. The organic layers were washed with brine, dried over Na_2SO_4, filtered and concentrated. The residue was purified by chromatography on silica gel to afford the desired product.

3. Results and discussion

At the onset of this study, we used the substrate **1a** and 4-CN-pyridine **2a** as the starting materials in electrolysis. With a Zn anode and graphite felt cathode, $PdCl_2$ worked as the catalyst precursor with diverse phosphine ligands (Scheme 2). It was found that the mono-dentate ligands **L1-L4**, regardless of triaryl or trialkyl phosphine, did not give any detectable branched products **3a** and linear **3a'**, and allyl acetate **1a** was recovered quantitatively. In addition, Pd precipitate was observed, suggesting that these phosphine ligands were not adequate to stabilize the Pd cation against cathodic reduction. When diphosphine ligand dppm **L5** was used, only trace amounts (<10% of GC yield) of products **3a** were detected. Then, dppe **L6** was evaluated, and the 5-membered-ring Pd complex did not give a significant boost to yield. If a dppp **L7**-Pd complex was applied, the yield of **3a** was dramatically improved to 64% GC yield and 60% isolated yield with a branch/linear ratio of 5:1. Further increasing the ring size of the complex by using dppb **L8** led to **3a** in an inferior yield of 45% and a B/L of 4:1. Highly rigid ligand **L9** gave a 67% GC yield and a 3:1 B/L ratio. However, a similar ligand **L10** failed to give decent results due to the lability of the alkene. We presume that ortho-chelation is necessary to achieve the transformation, and turned to evaluate **L11-L15**. The

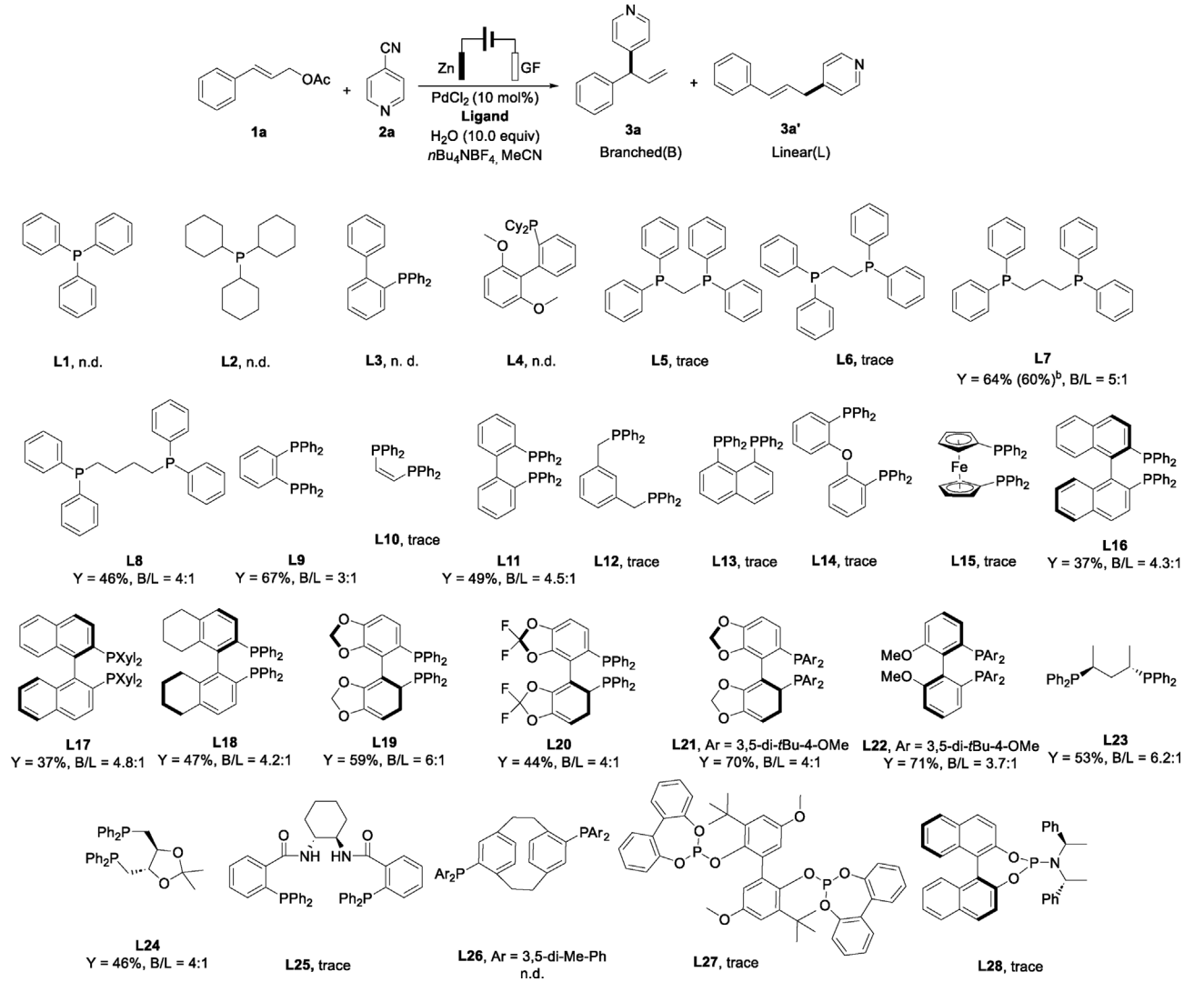

*Scheme 2. Evaluation of P ligands on the reactivity and selectivity of Pd-catalyzed electrochemical allyl pyridinylation. [a]Standard condition: **1a** (0.2 mmol), **2a** (0.6 mmol), $PdCl_2$ (10 mol%), diphosphine **L** (12 mol%)/monophosphine **L** (24 mol%), H_2O (10 equiv), MeCN (6 mL), nBu_4NBF_4 (0.1 mmol), 20 $mA{\cdot}cm^{-3}$, 4 hours, 35 °C, GC yield of **3a** with internal standard. [b]Isolated yield of **3a**.*

Table 1. Optimization of the other reaction parameters[a].

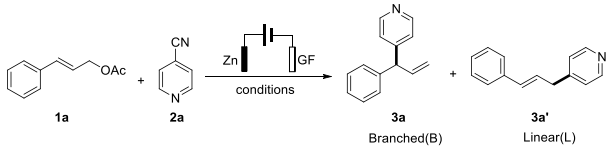

Entry	Deviation from standard conditions	Yield of **3a**	B/L
1	none	64%	5:1
2	no electricity	Nd	–
3	no $PdCl_2$	Nd	–
4	no ligand	Nd	–
5	no H_2O	Nd	–
6	graphite felt as anode	Trace	–
7	$LiClO_4$ instead of nBu$_4$NBF$_4$	Trace	–
8	DMF instead of MeCN	60%	2:1
9	DMSO instead of MeCN	48%	2:1
10	MeCN/MeOH (5:1, *v*/*v*)	74% (72%)[b]	5:1
11	Cinnamyl bromide instead of **1a**	Nd	–
12	Cinnamyl methyl carbonate instead of **1a**	Nd	–

[a] Standard conditions: **1a** (0.2 mmol), **2a** (0.6 mmol), $PdCl_2$ (10 mol%), **L7** (12 mol%), H_2O (10 equiv), MeCN (6 mL), nBu$_4$NBF$_4$ (0.1 mmol), 20 mA·cm^{-3}, 4 hours, 35 °C.
[b] Isolated yield in brackets.

ortho diphosphine **L11** worked as expected to offer **3a** in 49% yield. **L12-L15** with distal coordinative sites, intending for para-chelation, failed to give appreciable yields. Several axial ligands **L16-L19** with varied dihedral angles, which are proportional to the biting angle, were screened. It was found that the BINAP **L16**, XylBINAP **L17** and H8-BINAP **L18** with larger dihedral angles among the four ligands offered **3a** in 37%, 37% and 47% yields, respectively. By using ligands **L19** with smaller dihedral angles, the yield increased to 59%. By introducing electron-withdrawing backbone in **L20**, both the yield and B/L dropped slightly. Two chiral ligands **L21** and **L22** bearing bulky P-aryl groups could improve the yield further to 70%, however, the B/L dropped. A chiral version of dppp ligand **L23** also gave good yield for **3a** and a similar B/L ratio. DIOP **L24**, sharing the same ring size as dppb **L8**, provided almost identical results. Subsequently, the complex of Pd-Trost ligand **L25**, a widely applied diphosphine ligand for asymmetric allyl alkylation reactions, did not catalyze the transformation effectively. A highly rigid ligand, **L26**, gave neither **3a** nor **3a'** as the detectable products. Phosphite ligand **L24** and phosphamide **L25** were not valid ligands in this catalytic electrochemical allyl pyridinylation.

After identifying dppp with simple backbone as the ligand with balance of yield and B/L, we studied the impacts of other parameters on the yield of **3a** and the corresponding B/L ratio (Table 1). In comparison to the standard condition (Entry 1), the absence of electricity (Entry 2) or Pd salt (Entry 3) did not give any conversion. If **L7** was removed, metallic palladium precipitated from the solution (Entry 4). In addition, the proton source water was also necessary; otherwise, the reaction was completely shut down (Entry 5). Next, a sacrificial zinc anode was confirmed to be critical for this reductive cross coupling reaction (Entry 6). If $LiClO_4$ was applied as the supporting electrolyte instead of nBu$_4$NBF$_4$, the reaction did not proceed significantly (Entry 7). Other typical solvents, such as DMF (Entry 8) and DMSO (Entry 9), gave inferior yields. The GC yield was further increased to 74%, and the isolated yield was 72% (Entry 10). Finally, cinnamyl bromide (Entry 11) and cinnamyl carbonate (Entry 12) were not as competent as **1a** in the reaction, and did not give detectable **3a**.

With the optimum conditions being identified (Table 1, Entry 10), we started to explore the substrate scope with various allyl acetates and 4-CN-pyridines without or with a second substituent group (Scheme 3). First, several substituted cinnamyl acetates were subjected to this Pd-catalyzed reaction. In the series of products **3b** to **3g**, the isolated yields ranged from 45% to 71%. Generally, the B/L did not vary much between 3:1 and 6:1. Epoxide (**3f**) and TMS-acetylenyl (**3g**) were compatible with the reaction conditions. Relatively low yields were observed when meta-substitutions were presented in the products **3h** to **3j**. On the other hand, the B/L remained at approximately 4:1. In the case of products **3k**—**3n** bearing *para* electron-donating groups, the isolated yields were relatively high. Next, the products **3o**—**3v** incorporating internal allyl groups were also prepared well with the identical protocol. We presumed that the B/L was

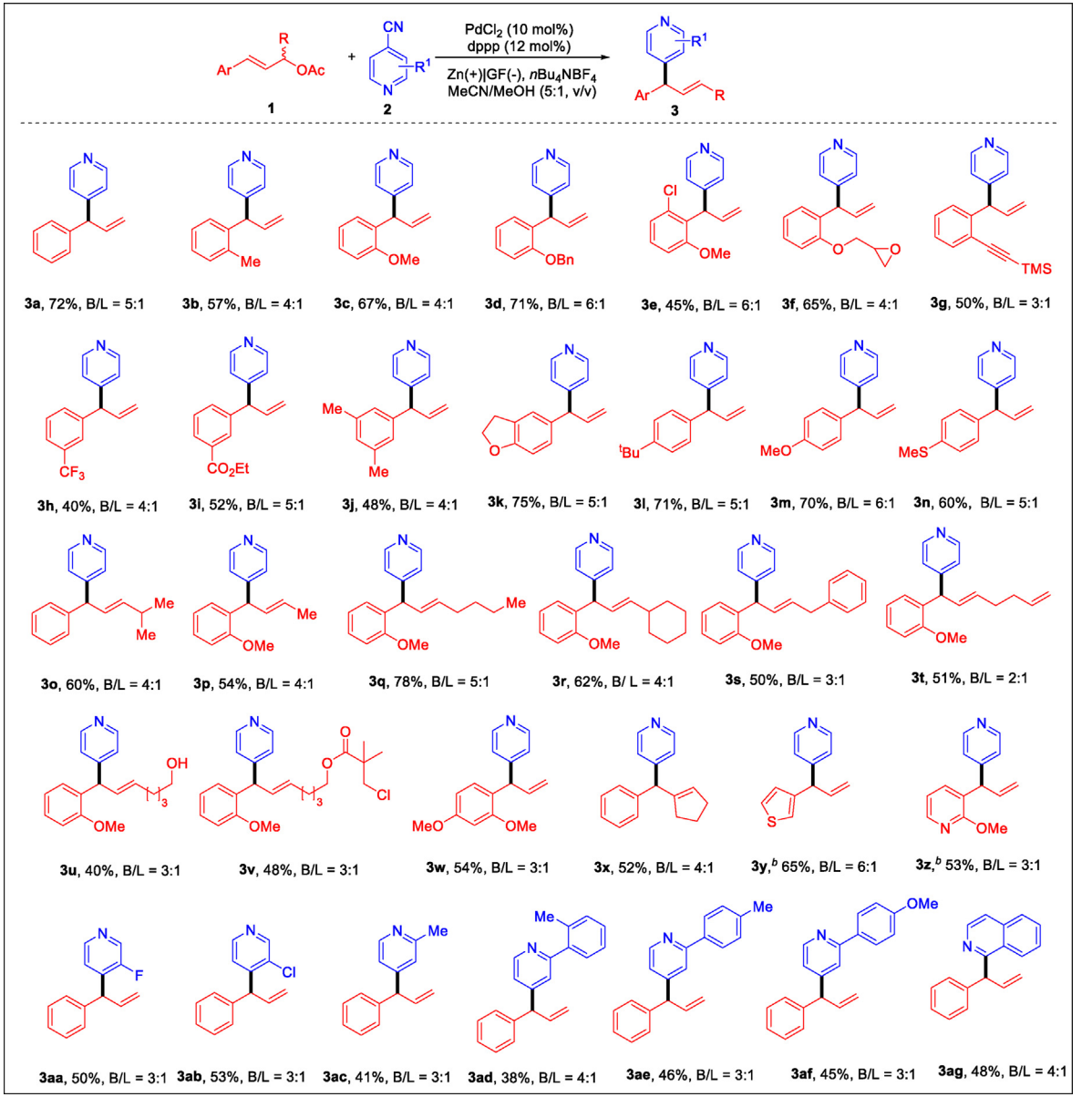

Scheme 3. Substrate scope of Pd-dppp-catalyzed electrochemical allyl pyridinylation.

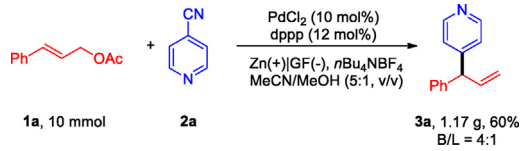

Scheme 4. Gram scale synthesis of product 3a.

determined by the ligands, since different combinations of carbon chains in the substrates **1o**−**1v** did not alter it too much. A branched product **3w** bearing two methoxy group was isolated in 54% yield from a reaction of B/L = 3:1. In a substrate **1x** bearing a cyclic allyl acetate gave the target product

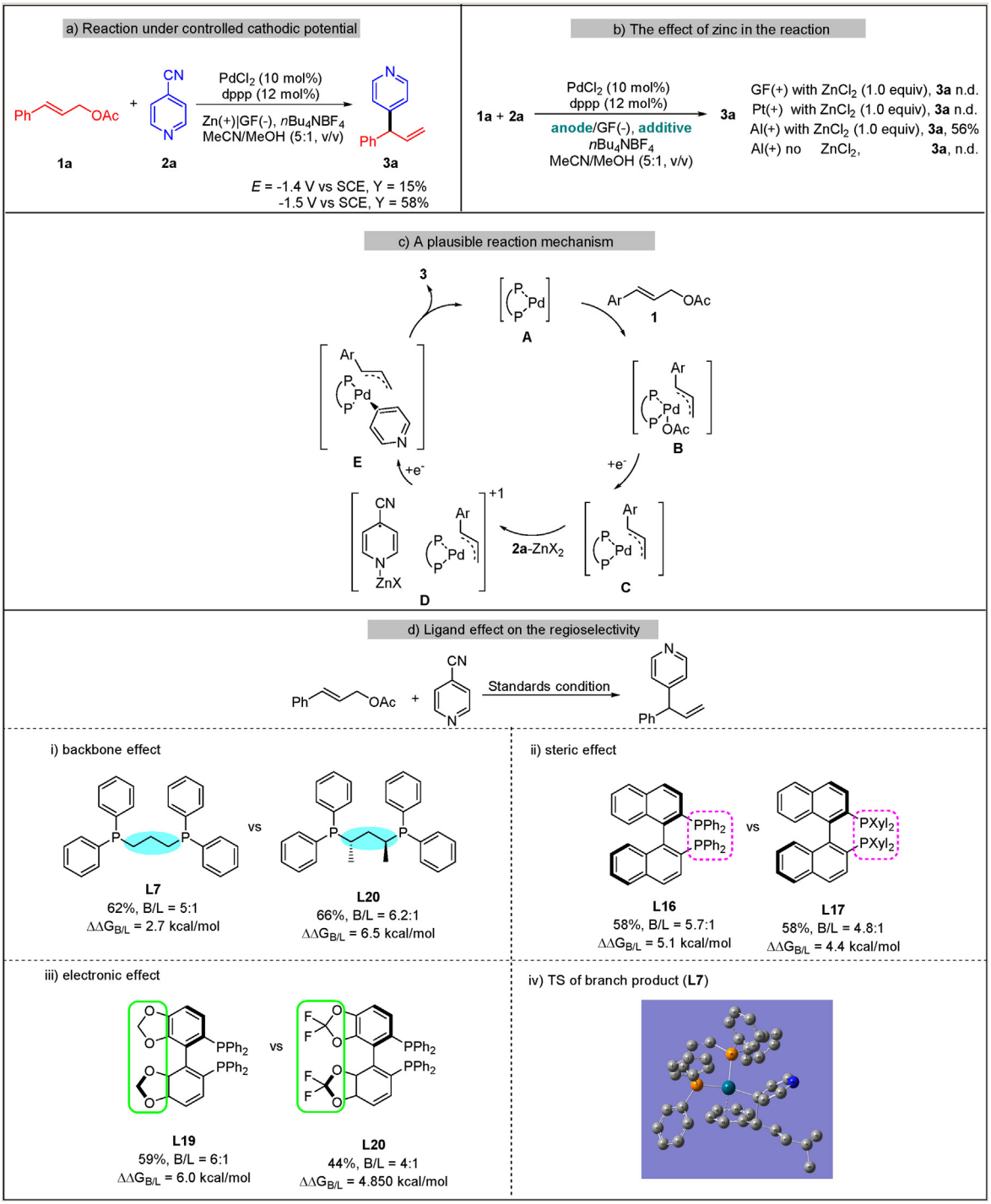

Scheme 5. Controlled reaction and a plausible reaction pathway.

3x in 52% isolated yield and a 4:1 B/L. Two substrates bearing heterocycles **1y** and **1z** smoothly gave rise to the corresponding products **3y** and **3z** in 65% and 53% isolated yields, respectively. Subsequently, *N*-heterocycles with cyano substitution other than **2a** were examined with **1a** under the same conditions. It was found that the groups at the 2- or 3-position impacted the reactions to some extent. If a steric group was presented at the 3-position of pyridine, the reaction did not proceed. Only the products with 3-fluoro (**3aa**) or 3-chloro (**3ab**) pyridinyl groups were generated in 50% or 53% isolated yields at a B/L ratio of 3:1. It was found that the alkyl or aryl group at the 2-position of CN-pyridine allowed the desired conversion, although the yields of **3ac**−**3af** were generally lower than that of **3a**. Meanwhile, the B/L ratio remained at a similar level. In addition, one example using 1-CN-isoquinoline provided the product **3ag** in 48% isolated yield. In this substrate scope list, the yield was the isolated yield of the branched product, and the B/Ls were characterized from the ^{1}H NMR of the crude mixture. Generally, the overall yields of B+L were 80%−90%, along with hydrode-acetate byproducts, for example, allylbenzene from the substrate **1a**.

Next, we explored the potential of this Pd-catalyzed allyl pyridinylation reaction at the gram scale (Scheme 4). The reaction proceeded smoothly, generating the product **3a** in 60% yield, and the B/L remained at the same level.

Subsequently, the reaction was controlled at −1.5 V vs. SCE under which neither allyl acetate **1a** nor 4-CN-pyridine **2a** could be reduced directly at the cathode. The reaction smoothly produced **3a** in almost identical yield to that under the standard conditions (Scheme 5a). This phenomenon implied a mediated process operated in the reaction. Afterwards, the effect of zinc anode was investigated with different combinations of anodes and additives (Scheme 5b). With the stoichiometric $ZnCl_2$ as the additive, changing a zinc anode to a graphite felt or a platinum, the desired product **3a** was not detected. If an aluminum anode was applied in the presence of stoichiometric $ZnCl_2$ as the additive, the reaction gave the desired product **3a** in the similar yield to that obtained under the standard conditions. However, the aluminum anode along did not offer **3a**. According to the reported works and the results in this work, a plausible reaction pathway is proposed in Scheme 5c. First, the $PdCl_2$/dppp complex is reduced at the cathode and enters the catalytic cycle with the oxidative addition of **1** to Pd species **A** as the initial step. Next, the intermediate **B** receives one electron from the cathode to form the formal Pd^{I} complex **C**, which acts as an electron shuttler to zinc-activated **2a**. Subsequently, the Pd species in the intermediate **D** receives and relays one electron to the adsorbed pyridinyl radical species. By losses of the zinc cation and CN anion, the allyl-Pd-pyridinyl complex **E** was formed. Finally, the reductive elimination from **E** produces the product **3** and regenerates the Pd catalyst **A**. It was shown that different ligands play important roles in regulating the regioselectivity. To gain some information on this effect, the DFT computation study was conducted to compare the different transition states during the formations of branch and linear products (Scheme 5d). At first, the standard ligand **L7** is compared with its variant (*S*,*S*)-**L20** to study the effect of ligand's backbone. It was found the transition states involving **L7** to the branch and linear products **3a** and **3a'** had a difference in the free energy change ($\Delta\Delta G$) of 2.7 kcal/mol, while 6.5 kcal/mol involving **L20**. Though the data do not fully fit the B/L ratios of **L7** and **L20**, the trend is consistent. Next, the steric effect was examined with BINAP **L16** and xyl-BINAP as the model ligand. The computational results show that the $\Delta\Delta G$ is also parallel to B/L ratios from both reactions. Accordingly, the electronic effect on the selectivity of B/L is explored by calculations with **L19** and **L20**, exhibiting the similar results. Based on these finding, we have proposed the backbone, steric and electronic influences on the regio-selectivity. Furthermore, to understand why branch products are the major outcome, the transition states to **3a** with **L7** ligands are analyzed. It was demonstrated that the aryl group participate the coordination to Pd, favoring the reductive elimination at the branch position.

4. Conclusions

In summary, a work on a Pd-catalyzed electrochemical allyl pyridinylation reaction was reported with the extensive evaluations of various P ligands. It was found that the electron-rich diphosphine ligands are necessary. More than 30 examples of isolated branched pyridinylation products were demonstrated. A reaction pathway involving the Pd-phosphine complex as both the transition metal catalyst and electron shuttler was proposed.

Conflict of interest

The authors decline no competing interest.

Acknowledgements

This work was supported by the National Natural Scieence Foundation of China (Nos. 22031008 and 22071105).

References

[1] Ataf A A, Adnan S, Zarif G, Nasir R, Amin B, Bhajan L, Ezzat K. A review on the medicinal importance of pyridine derivatives[J]. J. Drug Des. Med. Chem., 2015, 1(1): 1−11.

[2] Nakao Y, Yada A, Satoh J, Ebata S, Oda S, Hiyama T. Arylcyanation of norbornene and norbornadiene catalyzed by nickel[J]. Chem. Lett., 2006, 35(7): 790−791.

[3] McNally A, Prier C K, MacMillan D WC. Discovery of an α-amino C−H arylation reaction using the strategy of accelerated serendipity[J]. Science, 2011, 334(6059): 1114−1117.

[4] Pirnot M T, Rankic D A, Martin D BC, MacMillan D WC. Photoredox activation for the direct β-arylation of ketones and aldehydes[J]. Science, 2013, 339(6127): 1593−1596.

[5] Qvortrup K, Rankic D A, MacMillan D WC. A general strategy for organocatalytic activation of C-H bonds via photoredox catalysis: Direct arylation of benzylic ethers[J]. J. Am. Chem. Soc., 2014, 136(2): 626−629.

[6] Cuthbertson J D, MacMillan D WC. The direct arylation of allylic sp3 C−H bonds via organic and photoredox catalysis [J]. Nature, 2015, 519(7541): 74−77.

[7] Lipp B, Lipp A, Detert H, Opatz T. Light-induced alkylation of (hetero)aromatic nitriles in a transition-metal-free C-C-bond metathesis[J]. Org. Lett., 2017, 19(8): 2054−2057.

[8] Lima F, Kabeshov M A, Tran D N, Battilocchio C, Sedelmeier J, Sedelmeier G, Schenkel B, Ley S V. Visible light activation of boronic esters enables efficient photoredox $C(sp^2)$−$C(sp^3)$ cross-couplings in flow[J]. Angew. Chem. Int. Ed., 2016, 55(45): 14085−14089.

[9] Lipp B, Nauth A M, Opatz T. Transition-metal-free decarboxylative photoredox coupling of carboxylic acids and alcohols with aromatic nitriles[J]. Org. Chem., 2016, 81(15): 6875−6882.

[10] Gao L Z, Wang G Q, Cao J, Chen H, Gu Y M, Liu X T, Cheng X, Ma J, Li S H. Lewis acid-catalyzed selective reductive decarboxylative pyridylation of N-hydroxyphthalimide esters: Synthesis of congested pyridine-substituted quaternary carbons[J]. ACS Catal., 2019, 9(11): 10142−10151.

[11] Shi J L, Yuan T, Zheng M F, Wang X C. Metal-free heterogeneous semiconductor for visible-light photocatalytic decarboxylation of carboxylic acids[J]. ACS Catal., 2021, 11(5): 3040−3047.

[12] Wang G Q, Cao J, Gao L Z, Chen W X, Huang W H, Cheng X, Li S H. Metal-free synthesis of C-4 substituted pyridine derivatives using pyridine-boryl radicals via a radical addition/coupling mechanism: A combined computational and experimental study[J]. J. Am. Chem. Soc., 2017, 139(10): 3904−3910.

[13] Zhang X, Yang C, Gao H, Wang L, Guo L, Xia W J. Reductive arylation of aliphatic and aromatic aldehydes with cyanoarenes by electrolysis for the synthesis of alcohols[J]. Org. Lett., 2021, 23(9): 3472−3476.

[14] Ding W J, Sheng J, Li J, Cheng X. Electroreductive 4-pyridylation of unsaturated compounds using gaseous ammonia as a hydrogen source[J]. Org. Chem. Front., 2022, 9(10): 2634−2639.

[15] Cao J, Wang G Q, Gao L Z, Chen H, Liu X T, Cheng X, Li S H. Perfluoroalkylative pyridylation of alkenes via 4-cyanopyridine-boryl radicals[J]. Chem. Sci., 2019, 10(9): 2767−2772.

[16] Chen J, Zhu S Q, Qin J, Chu L L. Intermolecular, redox-neutral azidoarylation of alkenes via photoredox catalysis [J]. Chem. Commun., 2019, 55(16): 2336−2339.

[17] Lipp B, Kammer L M, Kücükdisli M, Luque A, Kühlborn J, Pusch S, Matuleviciute G, Schollmeyer D, Sackus A, Opatz T. Visible light-induced sulfonylation/arylation of styrenes in a double radical three-component photoredox reaction[J]. Chem. Eur J., 2019, 25(38): 8965−8969.

[18] Zhu S Q, Qin J, Wang F, Li H, Chu L L. Photoredox-catalyzed branch-selective pyridylation of alkenes for the expedient synthesis of Triprolidine[J]. Nat. Commun., 2019, 10: 749.

[19] Betori R C, Scheidt K A. Reductive arylation of arylidene malonates using photoredox catalysis (Retracted Article)[J]. ACS Catal., 2019, 9(11): 10350−10357.

[20] Qi J, Zhang F L, Jin J K, Zhao Q, Li B, Liu L X, Wang Y F. New radical borylation pathways for organoboron synthesis enabled by photoredox catalysis[J]. Angew. Chem. Int. Ed., 2020, 59(31): 12876−12884.

[21] Zhang S, Li L J, Li X R, Zhang J Q, Xu K, Li G G, Findlater M. Electroreductive 4-pyridylation of electron-deficient alkenes with assistance of $ni(acac)_2$[J]. Org. Lett., 2020, 22(9): 3570−3575.

[22] Li Y J, Han C J, Wang Y Y, Huang X, Zhao X W, Qiao B K, Jiang Z Y. Catalytic asymmetric reductive azaarylation of olefins via enantioselective radical coupling[J]. J. Am. Chem. Soc., 2022, 144(17): 7805−7814.

[23] Miao M, Liao L L, Cao G M, Zhou W J, Yu D G. Visible-light-mediated external-reductant-free reductive cross coupling of benzylammonium salts with (hetero)aryl nitriles[J]. Sci. China: Chem., 2019, 62(11): 1519−1524.

[24] Lehnherr D, Lam Y H, Nicastri M C, Liu J C, Newman J A, Regalado E L, DiRocco D A, Rovis T. Electrochemical synthesis of hindered primary and secondary amines via proton-coupled electron transfer[J]. J. Am. Chem. Soc., 2020, 142(1): 468−478.

[25] Wen J W, Yang X T, Yan K L, Qin H Y, Ma J, Sun X J, Yang J J, Wang H. Electroreductive C3 pyridylation of quinoxalin-2(1H)-ones: An effective way to access bidentate nitrogen ligands[J]. Org. Lett., 2021, 23(3): 1081−1085.

[26] Jahn U. Radicals in transition metal catalyzed reactions? Transition metal catalyzed radical reactions? A fruitful interplay anyway[J]. Top. Curr. Chem., 2011, 320: 323−451.

[27] Twilton J, Le C, Zhang P, Shaw M H, Evans R W, MacMillan D WC. The merger of transition metal and photocatalysis[J]. Nat. Rev. Chem, 2017, 1(7): 52.

[28] Lu J Q, Wang Y K, McCallum T, Fu N K. Harnessing radical chemistry via electrochemical transition metal catalysis[J]. iScience, 2020, 23(12): 101796.

[29] Cheng X, Lei A W, Mei T S, Xu H C, Xu K, Zeng C C. Recent applications of homogeneous catalysis in electrochemical organic synthesis[J]. CCS Chem., 2022, 4: 1120−1152.

[30] Ma C, Fang P, Liu Z R, Xu S S, Xu K, Cheng X, Lei A W, Xu H C, Zeng C C, Mei T S. Recent advances in organic electrosynthesis employing transition metal complexes as electrocatalysts[J]. Sci. Bull., 2021, 66(23): 2412−2429.

[31] Zhang W, Wang F, McCann S D, Wang D H, Chen P H, Stahl S S, Liu G S. Enantioselective cyanation of benzylic C−H bonds via copper-catalyzed radical relay[J]. Science, 2016, 353(6303): 1014−1018.

[32] Ge L, Zhou H, Chiou M F, Jiang H M, Jian W J, Ye C Q, Li X Y, Zhu X T, Xiong H G, Li Y J, Song L J, Zhang X H, Bao H L. Iron-catalysed asymmetric carboazidation of styrenes[J]. Nat. Catal., 2021, 4(1): 28−35.

[33] Zhang C, Li Z L, Gu Q S, Liu X Y. Catalytic enantioselective $C(sp^3)$-H functionalization involving radical intermediates [J]. Nat. Commun., 2021, 12(1): 475.

[34] Zhou Q, Chin M, Fu Y, Liu P, Yang Y. Stereodivergent atom-transfer radical cyclization by engineered cytochromes P450[J]. Science, 2021, 374(6575): 1612−1616.

[35] Ding W J, Li M F, Fan J K, Cheng X. Palladium-catalyzed asymmetric allylic 4-pyridinylation via electroreductive substitution reaction[J]. Nat. Commun., 2022, 13(1): 5642−5652.

[36] Pitzer L, Schwarz J L, Glorius F. Reductive radical-polar crossover: Traditional electrophiles in modern radical reactions[J]. Chem. Sci., 2019, 10(36): 8285−8291.
[37] Wiles R J, Molander G A. Photoredox-mediated net-neutral radical/polar crossover reactions[J]. Isr. J. Chem., 2020, 60(3−4): 281−293.
[38] Sharma S, Singh J, Sharma A. Visible light assisted radical-polar/polar-radical crossover reactions in organic synthesis [J]. Adv. Synth. Catal., 2021, 363(13): 3146−3169.
[39] Jiao K J, Li Z M, Xu X T, Zhang L P, Li Y Q, Zhang K, Mei T S. Palladium-catalyzed reductive electrocarboxylation of allyl esters with carbon dioxide[J]. Org. Chem. Front., 2018, 5(14): 2244−2248.
[40] Zhang H H, Zhao J J, Yu S Y. Enantioselective allylic alkylation with 4-alkyl-1,4-dihydropyridines enabled by photoredox/palladium cocatalysis[J]. J. Am. Chem. Soc., 2018, 140(49): 16914−16919.
[41] Zhang H H, Zhao J J, Yu S Y. Enantioselective α-allylation of anilines enabled by a combined palladium and photoredox catalytic system[J]. ACS Catal., 2020, 10(8): 4710−4716.
[42] Zhang H H, Tang M H, Zhao J J, Song C H, Yu S Y. Enantioselective reductive homocoupling of allylic acetates enabled by dual photoredox/palladium catalysis: Access to C2-symmetrical 1,5-dienes[J]. J. Am. Chem. Soc., 2021, 143(32): 12836−12846.

钯催化电化学烯丙位 4-吡啶化反应中的配体作用研究

丁伟杰[a,b,*]，杨春晖[b]，冯钟涛[c]，陆仕荣[a]，程旭[b,*]
[a] 台州学院材料科学与工程学院，浙江 台州 318000，中国
[b] 南京大学化学化工学院，江苏 南京 210023，中国
[c] 新加坡南洋理工化学化工生物技术学院，新加坡 637371，新加坡

摘要

过渡金属络合物在电化学合成中获得了广泛的应用，其中配体对于络合物在电场中稳定性、催化活性以及选择性的影响还了解有限。4-氰基-吡啶作为一种高效吡啶化试剂，在自由基化学中获得广泛应用。在前期的工作中，我们实现了电化学条件下，手性双膦配体钯络合物催化 4-氰基-吡啶与烯丙基醋酸酯反应，构建了多种手性烯丙基吡啶化合物。我们发现双膦配体对反应有着关键的作用，决定着反应的活性、区域选择性和对映选择性。在本工作中，我们系统性地研究了多种双膦配体钯金属络合物，在烯丙基醋酸酯与氰基吡啶的电化学还原偶联过程中的性质。通过控制实验，电化学分析以及理论计算等方法，我们揭示了双膦配体对于络合物稳定性及反应区域选择性的影响。进而，我们发现在电场条件下存在一个非稳定价态的过渡金属络合物。这个非稳定价态的过渡金属络合物中，双膦配体可以将电荷和自旋密度分散于整个络合物之中，而不是局限于金属离子之上。这样，络合物既可以作为电子转移催化剂，也可以作为过渡金属催化剂，同时控制整个电子转移过程以及成键过程。我们认为这种配体与金属在电场条件下的非稳定价态络合物，展现了电化学条件下过渡金属催化的独特能力，这有助于发展未来的新型的电化学催化体系。同时，我们还发现锌电极至关重要，其不仅可以活化 4-氰基吡啶，还可以淬灭氰根离子，展现出 Lewis 酸性金属离子的特殊用途。

关键词：电化学；钯催化；膦配体；吡啶化；烯丙基